

Scaling Results for the Liquid Sheet Radiator (LSR)

(NASA-TM-102100) SCALING RESULTS FOR THE
LIQUID SHEET RADIATOR (LSR) : (NASA- Lewis
Research Center) 8 p

CSCL 20D

N89-25277

Unclassified
G3/20 0217230

Donald L. Chubb and Frederick D. Calfo
Lewis Research Center
Cleveland, Ohio

Prepared for the
24th Intersociety Energy Conversion Engineering Conference
cosponsored by the IEEE, AIAA, ANS, ASME, SAE, ACS, and AIChE
Washington, D.C., August 6-11, 1989



Scaling Results for the Liquid Sheet Radiator

Donald L. Chubb and Frederick D. Calfo
National Aeronautics and Space Administration
Lewis Research Center
Cleveland, Ohio 44135

ABSTRACT

Surface tension forces at the edges of a thin liquid ($\sim 100\mu\text{m}$) sheet flow result in a triangularly shaped sheet. Such a geometry is ideal for an external flow radiator. The experimental investigation of such sheet flows has been extended to large sheets (width= $W = 23.5\text{cm}$, length= $L \approx 3.5\text{m}$). Experimental L/W results are greater than the calculated results. However, more experimental results are necessary for a complete comparison. The calculated emissivity of a sheet of Dow-Corning 705 silicone oil, which is a low temperature (300-400K) candidate for a liquid sheet radiator (LSR), is greater than .8 for sheet thicknesses greater than $100\mu\text{m}$.

1. Introduction

The liquid sheet radiator (LSR) is an external flow radiator similar in several ways to other external flow radiators such as the liquid droplet [1] (LDR) and liquid belt [2] radiators. All of these radiator concepts potentially have lower mass than solid wall radiators such as pumped loop and heat pipe radiators. They are also nearly immune to micrometeoroid penetration. However, the LSR has the added advantage of simplicity. Surface tension causes a thin ($\sim 100\mu\text{m}$) liquid sheet to coalesce to a point (Figure 1). As a result, the sheet flow has a triangular shape. Such a triangular sheet is desirable since it allows collection of the flow at a single point. To obtain a similar triangular area for the LDR requires very accurate aiming of many (10^3 - 10^6) droplet streams. Simplicity of the LSR should also result in lower mass for the LSR compared to the LDR and liquid belt radiators.

A major problem for all external flow radiators is the requirement that the working fluid be of very low ($\sim 10^{-8}$ TORR) vapor pressure in order to keep evaporative losses low. As a result,

working fluids are limited to certain oils (such as used in diffusion pumps) for low temperatures (300-400K) and liquid metals for higher temperatures [1]. Also, for the LSR to become a practical device large ($W \approx 3.5\text{m}$ in figure 1) sheet flows must be maintained. It is therefore necessary to understand the fluid mechanics of large sheet flows.

In the past only small ($W \leq 3.4\text{ cm}$) sheet flows have been investigated [3]. The major conclusions of that study were that the sheet length to width ratio, L/W , was a linear function of the flow velocity and that the flow was stable. Stability of the flow may seem surprising since surface tension dominated cylindrical flow breaks up into droplets as a result of the Rayleigh instability [4]. However, sheet flows remained stable even when acoustic oscillations were introduced in the flow [3].

A new facility now makes it possible to investigate larger ($W \leq 23.5\text{ cm}$) sheet flows. The major objective of this study is to determine the L/W scaling for these large sheets. Also a theoretical prediction for L/W scaling will be compared with the experimental results. Finally the emissivity of Dow-Corning 705 oil is calculated from experimental transmittance data.

2. Theoretical L/W Scaling

Figure 1 is a schematic drawing of a liquid sheet flow. Surface tension forces at the two edges of the sheet push the edges toward the z axis. As a result, as the flow moves in the z direction the edge cross-sectional area, A_c , grows. In order to satisfy mass continuity the edges approach each other and finally meet at the point $z = L$.

In a previous analysis [3] it was assumed that the edge cross-sectional areas, A_c , were cylinders. However, it is not necessary to make this assumption to calculate the velocity, v_e , at which the edges approach the z axis. Referring to figure 1(b) and neglecting any curvature of the sheet in the $y-z$ plane, the surface tension force on the infinitesimal surface area $dldz$ is

$$dF = -\frac{\sigma}{R_c} dl dz \quad (1)$$

where σ is the surface tension and R_c is the radius of curvature of the liquid-vacuum interface. The component of the force in the x direction is

$$dF_x = -\frac{\sigma}{R_c} \sin\Phi dl dz = -\frac{\sigma}{R_c} dy dz \quad (2)$$

and the radius of curvature is the following.

$$\frac{1}{R_c} = \frac{\frac{dy}{dx^2}}{\left[1 + \left(\frac{dy}{dx}\right)^2\right]^{3/2}} \quad (3)$$

Where $y(x)$ is the location of the vacuum-liquid boundary. Substituting eq. (3) in (2) and then integrating over the surface from $y = 0$ to $y = \tau/2$ will yield $1/2$ the x direction force on the sheet edge. Therefore, the total edge force in the x direction per unit length in the z direction is the following.

$$\frac{dF_x}{dz} = -2 \int_0^{\tau/2} \frac{\sigma \ddot{y}}{\left(1 + \dot{y}^2\right)^{3/2}} dy \quad (4)$$

Where, $\dot{y} = \frac{dy}{dx}$ and $\ddot{y} = \frac{d^2y}{dx^2}$. Making the substitution $u = \dot{y}$ in eq. (4) yields,

$$\frac{dF_x}{dz} = -2\sigma \int_{-\infty}^0 \frac{u}{\left(1+u^2\right)^{3/2}} du \quad (5)$$

so that,

$$\frac{dF_x}{dz} = 2\sigma \quad (6)$$

The significance of this result is that dF_x is independent of the cross-sectional shape of the sheet. It applies as long as the edge cross-section has an infinite slope at the edge and zero slope where it joins the main sheet.

The x direction force given by eq. (6) can be used in the integrated momentum equation for the control volume, defined by the left edge in

figure 1(b), to obtain the sheet edge velocity, u_e .

$$\rho\tau u_e^2 = \frac{dF_x}{dz} \quad (7)$$

Therefore,

$$u_e = \sqrt{\frac{2\sigma}{\rho\tau}} \quad (8)$$

This result shows that u_e will be constant if the sheet thickness, τ , remains constant. In the absence of gravity it can be shown that τ is a constant and that the sheet velocity in the z direction, w_0 , will also be a constant. With both u_e and w_0 constant the flow will form a triangular sheet, which agrees with experimental results.

For no gravity force the sheet flow will coalesce to a point at distance $z = L$ in the time, t_L , it takes the sheet edge to move the distance $W/2$.

$$t_L = \frac{W}{2u_e} = \frac{W}{2} \sqrt{\frac{\rho\tau}{2\sigma}} \quad (9)$$

Therefore, the sheet length, L , is the following,

$$L = w_0 t_L = \frac{Ww_0}{2} \sqrt{\frac{\rho\tau}{2\sigma}} \quad (10)$$

and

$$\frac{L}{W} = \sqrt{\frac{We}{8}} \quad (\text{no gravity force}) \quad (11)$$

where We is the Weber number.

$$We \equiv \frac{\rho\tau w_0^2}{\sigma} \quad (12)$$

Equation (11) says that in the absence of gravity L/W depends only on the Weber number. Also, for a given sheet thickness, L/W is a linear function of the sheet velocity, w_0 . In the experiments performed so far the gravity force has been in the direction of the flow (z direction). The importance of the gravity force [3] is determined by the Froude number, ($Fr = 2/\gamma_W$ in ref. 3)

$$Fr = \frac{w_0^2}{gW} \quad (13)$$

If Fr is large then the gravity force will have negligible effect on the sheet flow. For all

the experiments carried out so far, $Fr > 50$. Therefore, equation (11) should be adequate to predict the L/W scaling for this study.

3. Experimental Results

A schematic of the new experimental facility is shown in figure 2. It consists of a 30 cm inner diameter stainless steel pipe 3.5 m long. The axis of the pipe is aligned with the gravity field. Vacuum conditions exist inside the pipe with the pressure less than 10^{-2} TORR. At these conditions there will be negligible aerodynamic drag on the sheet flow. Flow of Dow Corning 705 silicone oil, ($\rho/\tau = 3 \times 10^{-2}$ sec 2 /cm 3), through the narrow slits is maintained by pressurizing a 40 gallon reservoir with nitrogen. (Nitrogen gas is separated from the oil by a diaphragm to prevent gas entering the oil.) The design of the slits is shown in figure 3. A length to width ratio, $L/W = 7$, was chosen to assure that fully developed laminar flow would result.

The flow velocity, w_0 , was determined from the measured volumetric flow rate, \dot{Q} , (m 3 /sec).

$$w_0 = \frac{\dot{Q}}{\tau W} \quad (14)$$

Flow rates were determined by measuring the pressure drop across a calibrated orifice in the supply line to the slits.

At this time only two slits have been investigated in the large facility. Both slits have a width, $W = 23.5$ cm. One slit has a thickness, $\tau = 150\mu\text{m}$, and the other has a thickness $\tau = 200\mu\text{m}$. The facility has windows at the top and bottom only. Therefore, the slit length, L , could be determined only for flows that went the length (~ 3.5 m) of the facility. A television camera on a translating table is now being installed in the facility. This will allow the measurement of all possible flow lengths.

Figure 4 shows the sheet flow produced by a $W = 3.4$ cm and $\tau = 109\mu\text{m}$ slit. As can be seen the sheet is triangular. The Froude number for this case is 370, so that the gravity effect is negligible. Therefore, eq. (8) indicates that the sheet edge velocity, u_e , and the flow velocity, w_0 should be constant. With u_e and w_0 both constant the predicted sheet shape is triangular, which is in agreement with the experimental results. With close inspection of figure 4 the growth of the sheet edge area, A_C , can be seen.

In figure 5 the experimental results for L/W are plotted as a function of Weber number for three slit widths ($W = 2.54$ cm, 3.42 cm, and 23.5 cm). Also shown is the analytical result

given by equation (11). The experimental L/W results are larger than the predicted values. Part of the difference can be accounted for by the gravitational effect. The gravity force, which is neglected in equation (11), causes an increase in L. Of the data shown in figure 5 the point at $We \approx 970$ has the smallest Froude number ($Fr = 70$). Therefore, the largest discrepancy is expected for this point. More data for $We > 400$ will be obtained in the near future.

4. Sheet Emissivity

In reference 3 the following expression is given for the spectral emittance, ϵ_λ of an infinite sheet.

$$\epsilon_\lambda = 1 - \tau_\lambda = 1 - 2E_3(a_\lambda\tau) \quad (15)$$

Where τ_λ is the spectral transmittance, a_λ is the absorption coefficient and $E_3(x)$ is the exponential integral.

$$E_3(x) = \int_0^1 u \exp(-x/u) du \quad (16)$$

The total hemispherical emissivity is defined as the following [6],

$$\epsilon = \frac{\int_0^\infty \epsilon_\lambda e_{\lambda b}(\lambda, T) d\lambda}{\sigma_{SB} T^4} = 1 - \frac{2}{\sigma_{SB} T^4} \int_0^\infty E_3(a_\lambda\tau) e_{\lambda b} d\lambda \quad (17)$$

where $e_{\lambda b}$ is the black body hemispherical spectral emissive power [6], T is the temperature, λ is the wavelength, and σ_{SB} is the Stefan-Boltzmann constant (5.67×10^{-8} watts/m 2 K 4).

For the temperature range (300-400K) where the silicone oils can be used $e_{\lambda b} \rightarrow 0$ for $\lambda < 4$ m and also for $\lambda > 70$ m. Therefore, to calculate ϵ it is necessary to know a_λ only in the wavelength region $4 < \lambda < 70 \mu\text{m}$. Both spectral emittance and transmittance of thin films of the silicone oils have been measured in this wavelength region [7,8]. Transmittance data for a $100\mu\text{m}$ thick film of Dow-Corning 705 taken from ref. 7 are reproduced in figure 6a. To estimate ϵ for Dow 705 the spectral emittance, ϵ_λ (or transmittance, τ_λ) was approximated as being constant in nine different wavelength regions as shown in figure 6b. For $300 \leq T \leq 400$ K the maximum value of $e_{\lambda b}$ occurs in the $8.5 \leq \lambda \leq 10.5$ region where $e_{\lambda b} \rightarrow 1.0$. Therefore, a large value of ϵ can be expected in the $300 \leq T \leq 400$ K region. To make the estimate of ϵ conservative an arbitrary value of $\epsilon_\lambda = .99$ was chosen in the regions where $\epsilon_\lambda \rightarrow 1$, and for $\lambda < 5\mu\text{m}$ and $\lambda > 50\mu\text{m}$ $\epsilon_\lambda = 0$ was arbitrarily

ily chosen. Using the spectral emittance approximations shown in figure 6b the absorption coefficient, α_λ , was calculated using equation (15) for each of the nine wavelength regions. These values are shown in figure 6b. The emissivity can then be calculated using equation (17) and the tabulation of $\frac{1}{\alpha_{\text{sb}} T} \int e_\lambda d\lambda$ given in reference 6. This leads to the following results:

$$\begin{aligned}\epsilon(\tau) = 1 - 2 & \left[.022 + .071E_3(.0057\tau) + .211E_3(.0129\tau) \right. \\ & \left. + .579E_3(.035\tau) + .095E_3(.016\tau) \right] \quad (18a)\end{aligned}$$

$T=300K$

$$\begin{aligned}\epsilon(\tau) = 1 - 2 & \left[.045 + .161E_3(.0057\tau) + .255E_3(.0129\tau) \right. \\ & \left. + .433E_3(.035\tau) + .07E_3(.016\tau) \right] \quad (18b)\end{aligned}$$

$T=400K$

where τ is in μm . Results calculated using equations (18) are shown in fig. 7. As can be seen, for $\tau \geq 100\mu\text{m}$ the emissivity is greater than .8. The emissivity reaches a maximum of .96 for $T=300K$ and a maximum of .92 for $T=400K$ because α_λ has been assumed to be zero for $\lambda \leq 5\mu\text{m}$ and $\lambda \geq 50\mu\text{m}$.

5. Conclusion

Using a new facility, large (width, $W=23.5$ cm, length, $L \approx 3.5$ m) sheet flows have been investigated. Analytical results that neglect gravity predict $L/W \sim \sqrt{We}$, where We is the Weber number. The experimental values for L/W are larger than those predicted analytically. However, more experimental data is required for a complete comparison.

Total hemispherical emissivity for Dow-Corning 705 silicone oil was calculated using experimental spectral transmittance data. Results show that $\epsilon > .8$ for sheet thicknesses, $\tau \geq 100\mu\text{m}$ in the temperature range $300 \leq T \leq 400K$.

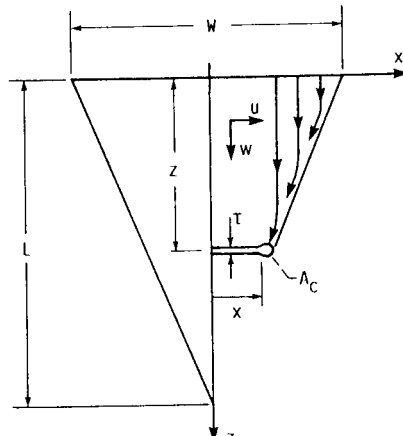
6. Acknowledgement

The authors wish to acknowledge William P. Lucas for setting up the experiment.

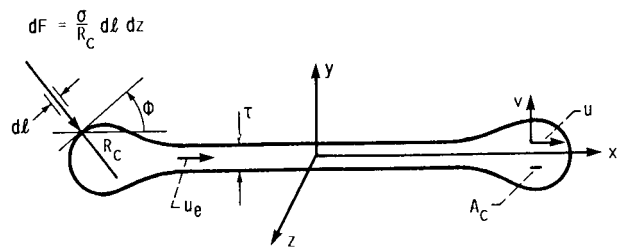
7. References

- Mattick, A. T. and Hertzberg, A., "Liquid Droplet Radiators for Heat Rejection in Space," Journal of Energy, Vol. 5, No. 6, Nov-Dec. 1951, pg. 387-393.

- Teagan, W. P. and Fitzgerald, K. "Preliminary Evaluation of a Liquid Belt Radiator for Space Applications," NASA CR-174807, 1984.
- Chubb, D. L. and White, K. A. III, "Liquid Sheet Radiator," AIAA 22nd Thermophysics Conference, Paper #87-1525 also NASA TM 89841 (1987).
- Drazin, P. G. and Reid, W. H., "Hydrodynamic Stability," Cambridge University Press (1981), pg. 22-27.
- Batchelor, G. K., "An Introduction to Fluid Dynamics," Cambridge University Press (1967), pg. 63.
- Siegel, R. & Howell, J. R., "Thermal Radiation Heat Transfer," second edition, Hemisphere Publishing Corp., Washington, DC, 1981, pg. 52.
- Mattick, A. T. & Hertzberg, A., "Liquid Droplet Radiator Performance Studies," Acta Astronautica, Vo. 12, pg. 591-598 (1985).
- Buch, R. R. & Huntress, A. R., "Organosiloxane Working Fluids for the Liquid Droplet Radiator," NASA CR-175033



(a) TOP VIEW OF SHEET FLOW.



(b) CROSS SECTION OF SHEET FLOW.

FIGURE 1. - Schematic of liquid sheet flow.

ORIGINAL PAGE
BLACK AND WHITE PHOTOGRAPH

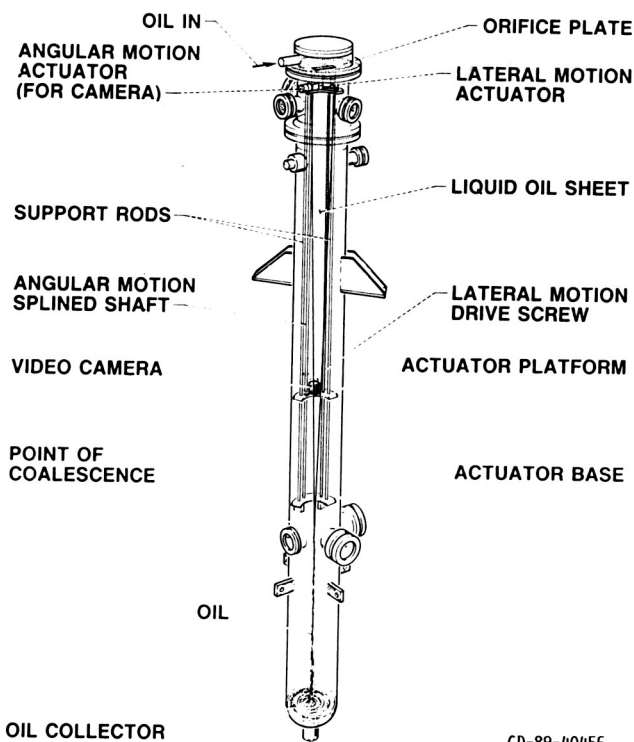
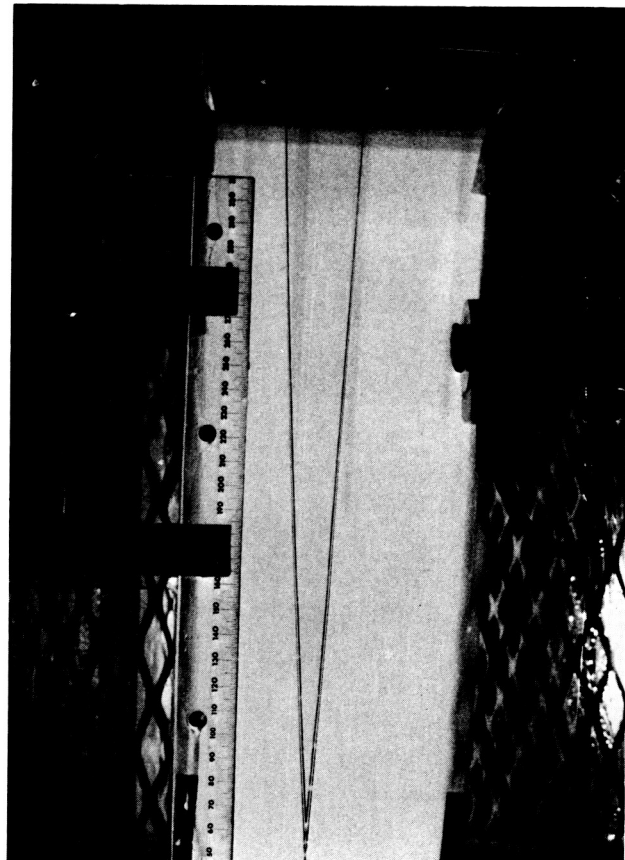


FIGURE 2. - SCHEMATIC OF EXPERIMENTAL FACILITY.



$\tau = 109 \mu\text{m}$, $l/\tau = 3.44$
 $L/W = 9.6$, $w_0 = 11.1 \text{ m/sec}$

FIGURE 4. - SHEET FLOW FROM A 3.4 CM WIDE SLIT.

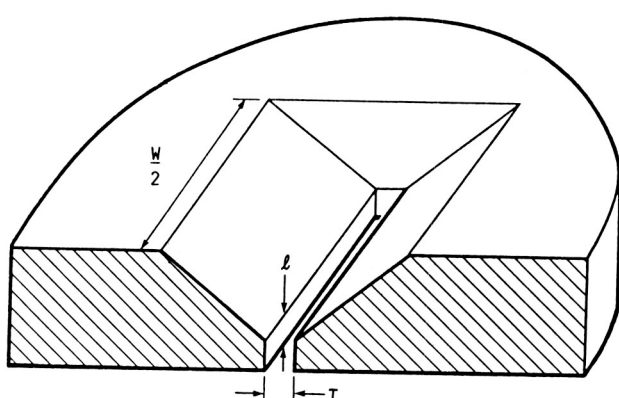


FIGURE 3. - TYPICAL SLIT PLATE FOR PRODUCING SHEET FLOW.

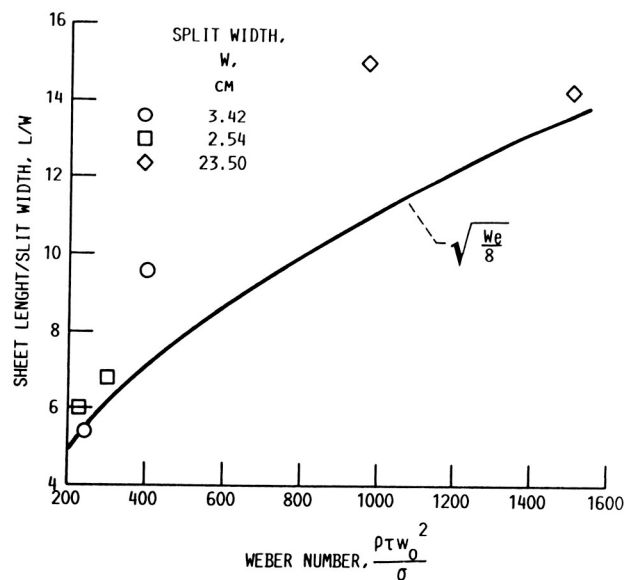
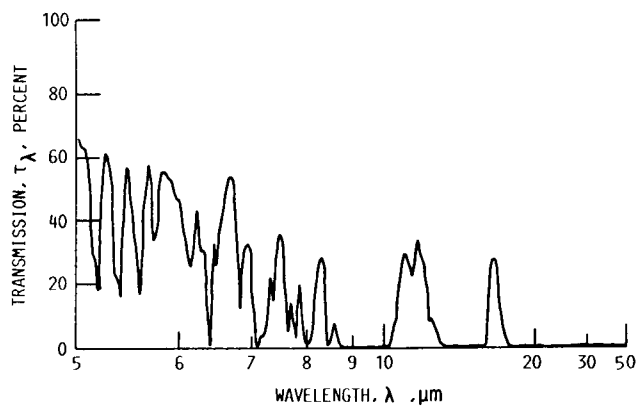


FIGURE 5. - SHEET FLOW L/W SCALING.



(a) TRANSMISSION DATA FOR $100\mu\text{m}$ THICK FILM.

WAVELENGTH RANGL. μm	SPECTRAL EMITTANCE $\epsilon_\lambda = 1 - \tau_\lambda$	ABSORPTION COEFFICIENT a_λ μm^{-1}
0 TO 5	0	0
5 TO 7	.60	.0057
7 TO 8.5	.85	.0128
8.5 TO 10.5	.99	.0350
10.5 TO 12.5	.85	.0128
12.5 TO 14	.99	.0350
14 TO 16	.90	.0160
16 TO 50	.99	.0350
50 TO ∞	0	0

(b) APPROXIMATION FOR a_λ FROM TRANSMISSION DATA.

FIGURE 6. - TRANSMISSION DATA FOR DOW-CORNING 705 OIL FROM REF. 7

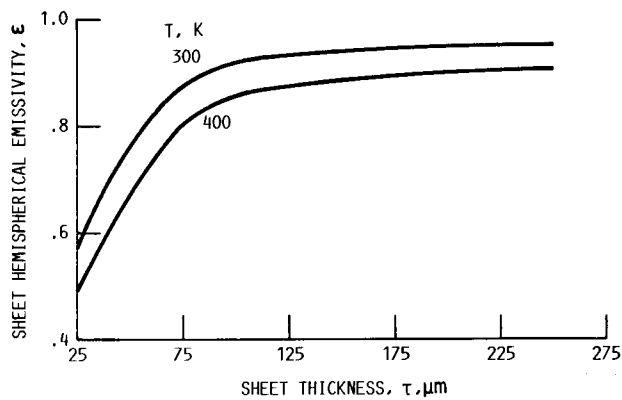


FIGURE 7. - EMISSIVITY OF DOW-CORNING 705 SHEET.



National Aeronautics and
Space Administration

Report Documentation Page

1. Report No. NASA TM-102100	2. Government Accession No.	3. Recipient's Catalog No.	
4. Title and Subtitle Scaling Results for the Liquid Sheet Radiator (LSR)		5. Report Date	
		6. Performing Organization Code	
7. Author(s) Donald L. Chubb and Frederick D. Calfo		8. Performing Organization Report No. E-4835	
		10. Work Unit No. 506-41-11	
9. Performing Organization Name and Address National Aeronautics and Space Administration Lewis Research Center Cleveland, Ohio 44135-3191		11. Contract or Grant No.	
12. Sponsoring Agency Name and Address National Aeronautics and Space Administration Washington, D.C. 20546-0001		13. Type of Report and Period Covered Technical Memorandum	
14. Sponsoring Agency Code			
15. Supplementary Notes Prepared for the 24th Intersociety Energy Conversion Engineering Conference cosponsored by the IEEE, AIAA, ANS, ASME, SAE, ACS, and AIChE, Washington, D.C., August 6-11, 1989.			
16. Abstract Surface tension forces at the edges of a thin liquid ($\sim 100 \mu\text{m}$) sheet flow result in a triangularly shaped sheet. Such a geometry is ideal for an external flow radiator. The experimental investigation of such sheet flows has been extended to large sheets (width = $W = 23.5 \text{ cm}$, length = $L \approx 3.5 \text{ m}$). Experimental L/W results are greater than the calculated results. However, more experimental results are necessary for a complete comparison. The calculated emissivity of a sheet of Dow-Corning 705 silicone oil, which is a low temperature (300-400K) candidate for a liquid sheet radiator (LSR), is greater than .8 for sheet thicknesses greater than $100 \mu\text{m}$.			
17. Key Words (Suggested by Author(s)) External flow radiator Thin film flow		18. Distribution Statement Unclassified—Unlimited Subject Category 20	
19. Security Classif. (of this report) Unclassified	20. Security Classif. (of this page) Unclassified	21. No of pages 8	22. Price* A02